JACS
JOURNAL OF THE AMERICAN CHEMICAL SOCIETY
pubs.acs.org/JACS
Article

Controlling the Dynamics of Ionic Liquid Thin Films via Multilayer Surface Functionalization

Boning Wu, John P. Breen, Xiangyu Xing, and Michael D. Fayer*

Cite This: J. Am. Chem. Soc. 2020, 142, 9482−9492
Read Online

ABSTRACT: The structural dynamics of planar thin films of an ionic liquid (IL) 1-butyl-3-methylimidazolium bis-(trifluoromethylsulfonyl)imide ($BmimNTf_2$) as a function of surface charge density and thickness were investigated using two-dimensional infrared (2D IR) spectroscopy. The films were made by spin coating a methanol solution of the IL on silica substrates that were functionalized with alkyl chains containing head groups that mimic the IL cation. The thicknesses of the ionic liquid films ranged from ∼50 to ∼250 nm. The dynamics of the films are slower than those in the bulk IL, becoming increasingly slow as the films become thinner. Control of the dynamics of the IL films can be achieved by adjusting the charge density on substrates through multilayer network surface functionalization. The charge density of the surface (number of positively charged groups in the network bound to the surface per unit area) is controlled by the duration of the functionalization reaction. As the charge density is increased, the IL dynamics become slower. For comparison, the surface was functionalized with three different neutral groups. Dynamics of the IL films on the functionalized neutral surfaces are faster than on any of the ionic surfaces but still slower than the bulk IL, even for the thickest films. These results can have implications in applications that employ ILs that have electrodes, such as batteries, as the electrode surface charge density will influence properties like diffusion close to the surface.

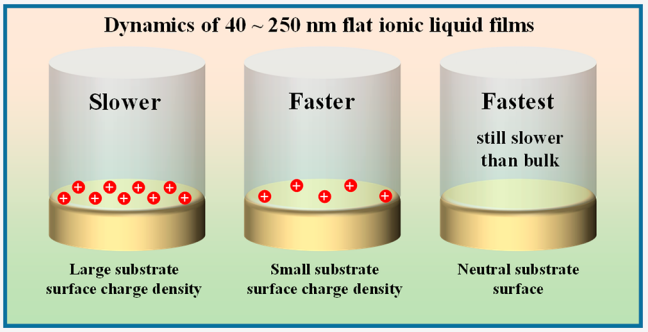

1. INTRODUCTION

Room temperature ionic liquids (ILs) are generally composed of bulky organic cations and either organic or inorganic anions.[1,2] The delocalization of charge among atoms of large cations and anions and their asymmetries reduce IL melting points below room temperature. ILs can be highly structured on mesoscopic distance scales due to the charge ordering, hydrophobic and hydrogen bonding interactions among the bulky ions. ILs are being used or investigated for a wide variety of applications.[3−7] In many of these applications, such as electrolytes in batteries,[8,9] solvents for CO_2 capture in supported ionic liquid membranes,[10−12] and media for biological studies,[13,14] the ILs are in contact with interfaces or confined on length scales from a few nanometers to almost a micrometer. The dynamics of ions in proximity to a charged interface play an important role in systems such as super capacitors[8] and batteries.[9] Therefore, understanding the dynamics of ILs at charged surfaces can be important in the development of such systems.[15]

The structural organization and dynamics of molecules at interfaces are different from those in the bulk liquid.[16−18] Molecules at interfaces generally display slower dynamics than those in the bulk liquid. Because the structure and dynamics of the interfacial IL layer are different from the bulk liquid, this layer affects the next layer of molecules, which in turn affects the next layer. In conventional liquids like water, this influence dies off rapidly. For example, water will display bulk dynamics by ∼2 nm or less from a surface, depending on the topography of the system.[19−22] However, bulk-like dynamics of ILs may not be observed even 100 nm from a surface.[23,24] The structural relaxation and solvation dynamics of ILs in the pores of poly(ether sulfone) membranes were investigated using two-dimensional infrared spectroscopy (2D IR)[25,26] and time dependent fluorescent Stokes shift measurements.[27] These experiments showed that the dynamics of ILs in the pores can be different from bulk IL dynamics even though the average pore size was ∼350 nm. It has been shown that the vibrational spectra of nearly 1 μm thick IL films supported by a silver plate are different from the bulk IL spectra.[28−30] Using a confocal microscope, the fluorescence anisotropy decay of fluorescent probes dissolved in ionic liquids were measured as a function of the distance from silica substrates. It was found that the anisotropy was not the same as the bulk until the focal point is hundreds of nanometers from the substrate.[31] Surface force

Received: March 18, 2020
Published: April 29, 2020

https://dx.doi.org/10.1021/jacs.0c03044
J. Am. Chem. Soc. 2020, 142, 9482−9492

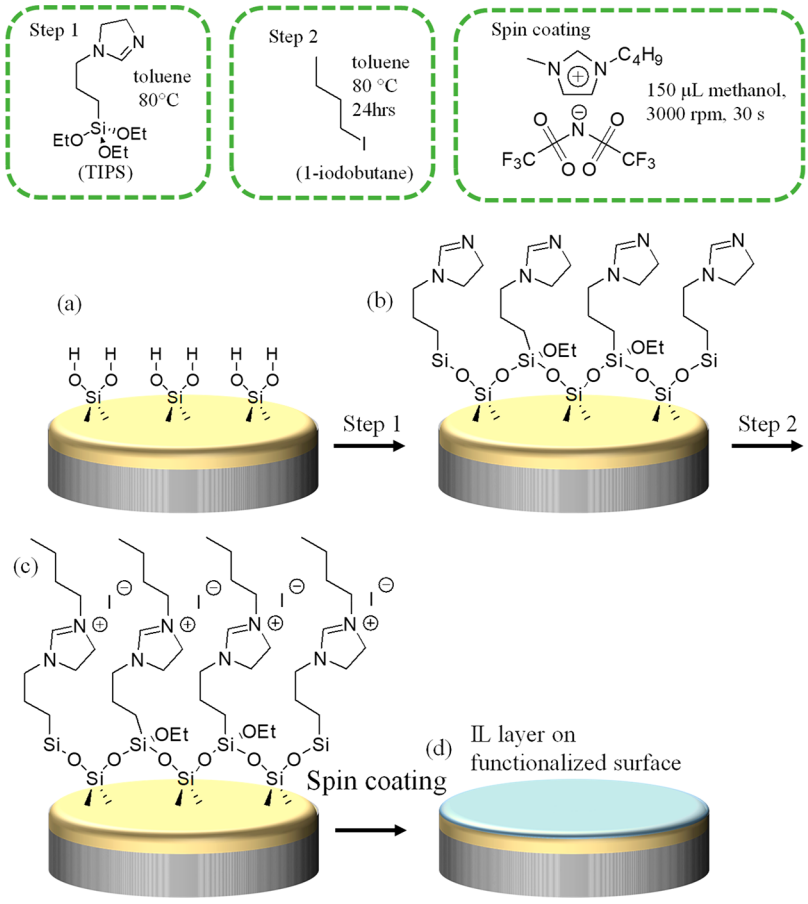

Figure 1. Schematic illustration of the preparation of the ionic liquid thin films with controlled thickness and surface charge density. (a) ∼100 nm thick SiO_2 on 3 mm thick CaF_2. (b) Substrates functionalized after step 1 with neutral imidazoline head groups. (c) Ionic monolayer/multilayer formed after reaction of imidazoline with iodobutane to give butylimidazolinium cationic head groups. (d) Ionic liquid thin film formed by spin coating the IL onto the functionalized surface. The actual reaction is more complicated than shown in this graphic; one, two, or three ethoxy groups from a particular triethoxyslilane can bind to the surface and cross-linking can occur to form a multilayer network.

apparatus (SFA) and atomic force microscopy (AFM) experiments show that ionic liquids exhibit nonbulk behavior under nanoconfinement for sizes that are 60−100 nm.[32−34] Molecular dynamics (MD) simulations have also shown long-range structural ordering in ILs and IL mixtures.[35−37]

To quantify the distance dependence of the influence of interfaces on ILs, a method for making <50 to 250 nm planar IL thin films was developed, and the film dynamics as a function of film thickness were investigated using two-dimensional infrared (2D IR) spectroscopy.[23,24] A ∼100 nm SiO_2 layer was first deposited on a 3 mm thick CaF_2 window. The surface of the SiO_2 layer was functionalized with an ionic layer that mimics the structure of the cation in the IL, e.g., $Bmim^+$ of 1-butyl-3-methylimidazolium bis-(trifluoromethylsulfonyl)imide ($Bmim^+$ NTf_2^-).[38] The films were prepared by spin coating a methanol solution of the IL on the functionalized substrate. (Details of the sample preparation are presented below.) The thicknesses of the films were controlled quantitatively by adjusting the concentration of the IL in the methanol solution. Substantially slower dynamics were observed in the films compared to the bulk liquid, with the dynamics becoming slower as the films became thinner.

In this paper, we report the control of the IL dynamics in films with a range of thicknesses by changing the surface charge density (density of cations) on the substrates. For a given film thickness, increasing the charge density slows down the dynamics. Zero charge density, made by functionalization surfaces with three different neutral head groups, produced the fastest dynamics, although still slower than the bulk IL liquid dynamics. Previous studies have shown that the slowing of dynamics in IL films involves charge ordering at and close to an interface.[24] Large charge density on a surface can slow the dynamics in films by both slowing the dynamics at the interfaces and extending the distance scale of the influence of the interface, since the range and magnitude of IL layering induced by an interface can be enhanced by a surface potential.[2]

At a solid-IL interface, with the solid substrate is immersed in the bulk IL, multiple layers of alternating cations and anions can be observed with AFM[2,39−43] and SFA[44−47] experiments, as well as simulations.[48−53] The AFM experiments found that applying a surface potential to the substrates increases the number of IL layers observed and the force needed by AFM tips to penetrate into the layers.[54,55] Increasing the surface voltage further increased the extent of the IL layering.[54−56] Changing the sign of applied surface potential interchanged the charge of the layer of the ions at the solid surface.[54,56−58]

In this work, grafting cationic groups onto substrates creates surface charge. The AFM and SFA experiments show changes in structure near the surface. The experiments presented here show changes in dynamics over distance from an interface on the order of 100 nm. The electric field produced by surface

https://dx.doi.org/10.1021/jacs.0c03044
J. Am. Chem. Soc. 2020, 142, 9482−9492

functionalization (1 electron per nm^2 creates an electric field of 2.8×10^{10} V/m) can be 1−2 orders of magnitude larger than those typically generated at the tip in a conductive AFM experiment. However, the higher charge densities are achieved by multilayer functionalization, and the *E*-field produced will be reduced by interspersed IL anions.

The dynamics of the ILs in thin films are measured using 2D IR spectroscopy,[59,60] which has been widely employed to study IL systems,[61−66] including thin films.[23,24] An IR probe, the CN stretch of SCN^-, dissolved in the IL has an inhomogeneously broadened absorption spectrum due to the different microenvironments in the vicinity of the probe. The 2D IR experiment reports on the time evolution of the liquid structure by measuring the time dependence of the 2D band shape. Liquid structural fluctuations cause changes in the vibrational frequencies of the probe molecules (spectral diffusion), which in turn result in increasing changes in the 2D band shape. Therefore, 2D IR spectroscopy provides a direct observable of liquid structure dynamics.

2. EXPERIMENTAL PROCEDURES

2.1. Sample Preparation. The method of surface functionalization is illustrated in Figure 1.[38] The surface charge density can be controlled by changing the extent of surface functionalization, which is related to the time that the substrate is immersed in a triethoxysilane solution during the surface functionalization.[67]

3-Thiocyanatopropyltriethoxysilane (80%), (chloromethyl)-triethoxysilane (96%), 3-(triethoxysilyl)propionitrile (97%), triethoxy(ethyl)silane (96%), and triethoxy-3-(2-imidazoline-1-yl)-propylsilane (TIPS, 97%), and 1-iodobutane (99%) were purchased from Sigma-Aldrich. Triethoxy(hexyl)silane (97%), triethoxy(octyl)-silane (97%), decyltriethoxysilane (98%), dodecyltriethoxysilane (93%), and *N*-[3-(triethoxysilyl)propyl]-1,2-ethanediamine (96%) were purchased from TCI America. CaF_2 windows, 1 in. diameter, coated with a 100 nm layer of SiO_2 on one surface were purchased from New Wave Optics. Ionic liquids ($BmimNTf_2$, 99%) and 1-butylmethylimidazolium thiocyanate (BmimSCN, 99%) were purchased from IoLiTec. Ethanol (200-Proof, 99.5%), toluene (99.9%), and methanol (extra dry, 99.8%) were obtained from Fisher Chemicals. Following the protocol developed over the past decade, the ionic liquids were dried under 100 mTorr vacuum at 80 °C for 48 h and stored in a N_2 purged glovebox before use. The drying procedure used here has been tested repeatedly with Karl Fischer titration to vet its efficacy and reproducibility, particularly on $BminNTf_2$.[27,65,66] The protocol results in a water content of less than 40 ppm. This low concentration of water has no effect on the measured IL dynamics.[68]

The surface functionalization utilizes the terminal OH groups on silica. The procedures for functionalizing charged surfaces and neutral surfaces are shown in Figures 1 and S3 (Supporting Information, SI), respectively. Functionalization to produce a charged surface requires 2 steps. Step 1 puts an alkyl chain with an imidazoline headgroup on the surface. Step 2 converts the imidazoline into the cation, imidazolinium. In step 1, a 100 nm layer SiO_2 coated CaF_2 window is immersed in a 0.8% (m/m) toluene solution of TIPS and refluxed at 80 °C. In step 2 the window is immersed in a 0.4% (m/m) toluene solution of 1-iodobutane and refluxed at 80 °C for 24 h. The surface coverage (charge density) is determined by the immersion time in step 1. Functionalization to produce a neutral surface only uses one step, in which an alkyl chain with the appropriate neutral headgroup is attached to the surface. This is done by immersing the window in a toluene solution of the corresponding triethoxysilane and refluxing at 80 °C for 24 h. After each immersion procedure, the solution is removed, the window is rinsed with toluene 3 times, sonicated in toluene for 5 min, followed by rinsing with ethanol 3 times, sonication in ethanol for 5 min, and drying using a clean nitrogen gas flow.

The samples were prepared in a nitrogen glovebox, where the water and oxygen levels are below 0.5 and 5 ppm, respectively. To make an ionic liquid thin film, 150 μL of methanol solution of IL is dropped on the center of a functionalized window, which is then spun at 3000 rpm for 30 s. IL thin films are formed when the methanol solvent evaporates. For the 2D IR samples, the vibrational probe SCN^- is added to the IL using a 1:10 (molar ratio) mixture of BmimSCN and $BmimNTf_2$ to make the precursor methanol solution. Thin films are sealed in a sample cell under an N_2 atmosphere by stacking a 1 in. diameter O-ring and another CaF_2 window on the top and sealed by tightening a retention ring. This preparation in the sample cell has been tested and shown to be airtight by observing the water hydroxyl stretch region with FT-IR for many days. Thus, atmospheric water is prevented from entering the sample.[69] In addition, FT-IR spectra were taken on each sample before and after the experiments, and no increase in water was observed. To make thin films of thickness near ~220 nm (1:10), ~120 nm (1:20), ~90 nm (1:28.5), ~50 nm (1:50), the concentrations of the IL in methanol are adjusted. The mass ratios between IL and methanol are shown in the parentheses.

The FT-IR spectra of the samples were taken using a Thermo Scientific Nicolet 6700 Fourier transform infrared (FT-IR) spectrometer. FT-IR spectra were used to determine the thicknesses of the films. The thicknesses were calculated by comparing the absorbance of C−H stretches between 3070 and 3210 cm^{-1} (from C−H bonds on the imidazolium ring) in the films with those in bulk IL samples of known thickness. By measuring the same sample multiple times, we determined that the error in the FT-IR measurement of the film thicknesses is ±5 nm.

This method is based on the extinction coefficients of the C−H absorption spectra being the same in the bulk and the films. Figure S7 shows a comparison of the C−H stretching region spectra for the bulk sample and high and low charge density film samples. These spectra are essentially identical. In particular, all of the peak positions are the same. The transition dipole, which determines the extinction coefficient, is given by the dipole derivative, i.e., the derivative of the potential around the potential minimum. The fact that the peak positions are the same means that the 0−1 vibrational transition frequencies are the same. The transition frequencies depend on the shape of the vibrational potential. If the shape changed in going from the bulk liquid to the films, the transition frequencies would be different. For the transition dipoles to change to any substantial extent, there would have to be a significant change in the shapes of the potentials, which would change the vibrational transition frequencies (spectroscopic peak positions). Since the peak positions are the same in the bulk liquid and films, the assumption that the extinction coefficients are the same is robust.

A Horiba XploRA Confocal Raman microscope was used to characterize the flatness of the films by measuring the Raman signal from IL on different spots. Images of samples were taken with a visible microscope using a 10× objective, and then the Raman spectra using a 532 nm laser were taken of the IL by scanning a range of spots with the confocal microscope using a 100× objective and a step size of 20 μm for a total length of 200 μm. The Raman signal from the N−S stretch of NTf_2^- at 740 cm^{-1} was measured at each spot, and the standard deviation of these measurements was used to determine the film thickness variation. It has been shown theoretically that a thickness variation of the film in the IR laser spot size, 100 μm, has almost no effect on the measured dynamics.[24] The visible images, Raman spectra, and integrated N−S stretch signal intensities of the films are shown in Figures S5 and S6 of the SI.

2.2. 2D IR Spectroscopy. The 2D IR spectra were measured using the same instrument as described previously.[23] A Ti:sapphire oscillator seeded a regenerative amplifier with a 3 kHz repetition rate. The 800 nm output pumped a home-built multistage optical parametric amplifier to obtain mid-IR that was centered at 2063 cm^{-1} and had a 95 cm^{-1} full width at half-maximum bandwidth. The 2D IR spectrometer is based on a germanium acousto-optic modulator pulse shaping system.[59] The phases and the delay time τ between pulse 1 and pules 2 were controlled using the pulse shaper. The delay time T_w between pulse 2 and pulse 3 was controlled with a mechanical delay line. The polarization was set to vertical (s-polarization) for the first two pulses, and horizontal (p-polarization)

https://dx.doi.org/10.1021/jacs.0c03044
J. Am. Chem. Soc. 2020, 142, 9482−9492

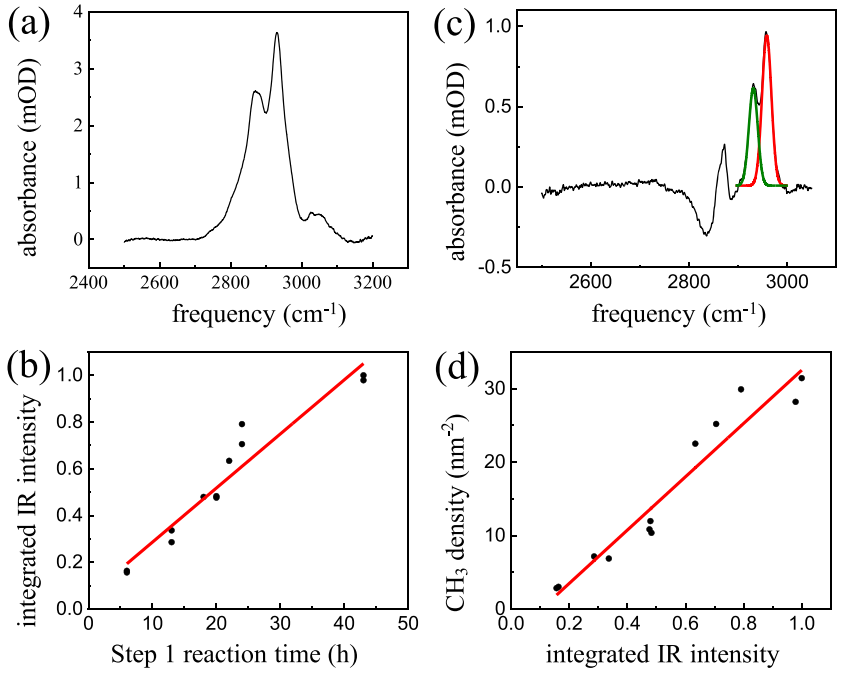

Figure 2. (a) FT-IR spectra of the functionalized neutral surface after step 1. (b) The integrated area of the spectrum in (a) vs the step 1 reaction time. (c) FT-IR spectrum of the surface after step 2 minus the spectrum after step 1. The green band is the absorption of the methylenes and the red band is the absorption of the terminal CH_3s on the butyl chains. (d) The surface CH_3 densities calculated from the integrated methyl peak intensity in panel c vs the integrated area in panel b. Only the butylimidazolinium cation head groups have methyl groups, so the surface density of methyls is the surface density of cations.

for pulse 3 which stimulates the emission of the horizontally polarized echo pulse. Pulse 3, which is the probe pulse, also acts as the self-heterodyned local oscillator (LO) for the echo and is collinear with the 2D IR vibrational echo signal. The probe pulse, modulated by the echo signal, is steered into a monochromator, and a 32-pixel MCT array detector was used to detect the heterodyned signal.

In a 2D IR experiment, the first pulse labels the initial frequencies of the probe molecules across the inhomogeneously broadened absorption spectrum. The second pulse stores the information. During the period T_w, the liquid structure evolves. The third pulse stimulates the emission of the echo pulse, which reads out the final frequencies of the probe molecules. At short T_w, there has been little time for the liquid structure to change, so the initial and final frequencies are highly correlated. As T_w increases, the liquid has more time to evolve in structure, and the final frequencies become less correlated with the initial frequencies. The loss of correlation causes the shape of the 2D spectrum to change. The frequency−frequency correlation function (FFCF) relates the experimental observables, i.e., the T_w dependent shapes of the 2D spectra, to the underlying dynamics of the system. The FFCF describes the loss of correlation among the initial and final frequencies. It is the time dependent correlation function of the initial and final frequencies, which can be written following Kubo as[59,70]

$$f(t) = \langle \delta\omega(0)\delta\omega(t)\rangle = \sum_i \Delta_i^2 \exp(-t/\tau_i) \quad (1)$$

where $\delta\omega(0)$ and $\delta\omega(t)$ are the instantaneous frequencies at time 0 and t, respectively. Δ_i and τ_i are the amplitude and time constant of the ith decay component of the frequency correlation, respectively. The bracket indicates an ensemble average over all probe frequencies. The Center Line Slope (CLS) method was used to obtain the normalized FFCF, CLS(T_w).[71,72] In eq 1, if $\Delta\tau \ll 1$ for one of the terms, this term is motionally narrowed and contributes to the homogeneous line width and does not have a T_w dependence. A measure of the homogeneous line width is the difference between 1 and the value of the CLS at $T_w = 0$. Using the CLS(T_w) and the linear absorption line shape, the full FFCF, including the homogeneous component, can be determined.[71,72]

In the experiments presented below, the bulk sample's 2D IR spectra were measured in the transmission geometry with nearly normal IR incident angles to the samples. Thin films were measured with the near-Brewster's angle reflection geometry method.[23,73] This method greatly enhances the amplitude of the signal field relative to the LO, producing high quality data in spite of the very thin samples. In the reflection geometry, pulse 3 (the probe pulse) had an incident angle of 52° (close to Brewster's angle), and the reflected combined signal/LO was steered into the monochromator/array detector. The signal to LO ratio was enhanced by a factor of 30 with the reflection geometry. In the reflection geometry, the sign of the 2D spectra is opposite of that in the transmission geometry.

3. RESULTS AND DISCUSSION

3.1. Sample Preparation and Characteristics. Methods for making IL films including vapor deposition on mica[74] and alumina,[75] dip-coating on silicon surface,[76] spin coating on Si(111),[77] and molecular beam deposition on various substrates[78] have been reported. However, some of these methods produced IL droplets instead of flat films.[74,76] It is more common to make IL films on metal surfaces. Ultrahigh vacuum physical vapor deposition methods are widely used to prepare ultrathin films up to a few IL monolayers on metal surfaces.[79−85] Thick IL films of ∼1 μm were made on silver substrates by spin coating[86] or dynamic wetting methods.[28−30]

Previously,[23,24] a method was developed to make thin films of ILs with controlled thickness by spin coating a methanol solution of the IL on a silica surface that has been functionalized with an ionic monolayer that mimics the cation of the IL.[38] After the methanol evaporates, the ionic liquid forms a flat thin film. The silica surface is a 100 nm thick layer on a 3 mm thick CaF_2 substrate to enable IR transmission.

https://dx.doi.org/10.1021/jacs.0c03044
J. Am. Chem. Soc. 2020, 142, 9482−9492

In this work, in addition to controlling the film thickness, we also achieved control of the surface charge density by adjusting the density of the surface functionalized ionic groups. The chemical processes are shown in Figure 1. The two steps are immersing the CaF_2/SiO_2 window in a toluene solution of triethoxy-3-(2-imidazoline-1-yl)propylsilane (TIPS) and then iodobutane. In both steps, the toluene was refluxed at 80 °C. During step 1, the triethoxysilyl groups react with the surface OH groups, and the alkyl chains with imidazoline head groups are grafted onto the surface (see Figure 1b). The FT-IR spectrum of the substrate after the step 1 deposition is shown in Figure 2a. The peaks between 2750 and 3010 cm^{-1} were integrated, and in Figure 2b the areas are plotted against the immersion time. The surface coverage increases as the immersion time increases, as has been reported previously.[67] The red line is a linear fit to the data. The high correlation between the peak intensity and immersion time shows that the surface density of neutral moieties deposited in step 1 can be controlled.

Step 2 (see Figure 1) converts the imidazoline groups into imidazolinium cations using the nucleophilic reagent iodobutane. Figure 2c shows the FT-IR spectrum that results from subtracting the spectrum of the substrate before step 2 from the spectrum after step 2. The red peak and the green peak are the asymmetric stretches from the butyl groups' CH_3 and CH_2 moieties, respectively. These two peaks are fit with Gaussian line shape functions, and the peak areas of CH_3 peaks are used to determine the density of terminal butyl groups, which is also the cation density or charge density bound to the surface. The CH_3 band extinction coefficient was determined by absorption measurements on bulk 1-iodobutane, and reasonably assuming that the transition dipole of the CH_3 asymmetric stretch of the butyl group of 1-iodobutane is the same as that of the CH_3 asymmetric stretch of the butyl group attached to imidazolinium. Polarization-selective FT-IR spectra of a functionalized substrate were taken. The functionalized substrate was measured with vertically and horizontally polarized IR beams at 0° and 40° incident angles. The IR peak shapes and intensities measured form the different polarizations and angles were all the same, demonstrating that the head groups do not have preferential orientations relative to the surface.

In Figure 2d, the number of methyl groups per unit area after step 2 is plotted against the integrated area of the 2750–3150 cm^{-1} region absorbance after step 1 (Figure 2A). The red line is a linear fit to the data. Each methyl corresponds to an imidazolinium cation. Any neutral imidazolines that did not react do not have a methyl moiety. The surface densities of imidazolinium cations range from 3 to 30 nm^{-2}. The value can be larger than the OH group density on the silica surface or the density of a triethoxysilane monolayer (~5 nm^{-2}).[87] It is well established that the reaction in step 1 can form a multilayer network because of cross-linking between triethoxysilyl groups.[88−90] While we use the term layers, the actual structure is probably better thought of as a cross-linked three-dimensional network rather than a stacked set of well-defined single layers. We roughly estimate the thicknesses of the surface functionalized multilayer to be between ~1 and ~5 nm, with the thickness increasing with the charge density, based on the thicknesses obtained by ellipsometry in a related system.[91]

After step 1 in the functionalization, the surfaces have neutral functionalization. After step 2, the head groups have been converted to cations with I^- counterions. After spin coating with $BminNTf_2$, the overwhelming number of NTf_2^- anions should result in NTf_2^- counterions for the butylimidazolinium cationic head groups. It is not known if there is complete charge balance in the surface functionalized layers. When we refer to charge density, it is a measure of the density of the cationic head groups.

For comparison to the measurements on the surfaces functionalized with the cationic butylimidazolinium head groups, surfaces were also functionalized with neutral groups, particularly chloromethyl (-MeCl), cyanoethyl (-EtCN), and ethyl (-Et). The surfaces were functionalized with these species by performing only step 1 with the appropriate triethoxysilyl-R reagents. Spin coating on surfaces functionalized with these species formed high quality very flat films with thickness variations of ~5%. A number of other neutral groups used for functionalization also formed high quality films, while others, particularly long alkyl chains, did not result in good spin coated films. These results are discussed in detail in the SI.

3.2. 2D IR Spectroscopy. The CN stretching mode of SCN^- anions was used as the vibrational probe. SCN^- anions were added in the form of BmimSCN, so only the anion is different. A 1:10 mixture of BmimSCN and $BmimNTf_2$ makes films of the same quality as pure $BmimNTf_2$, as shown in Figure S5 in the SI. Every ionic liquid thin film was inspected under a visible microscope after the 2D IR experiments and some were examined with the Raman microscope. All films on charged surfaces were still very flat after the measurements. However, although the thin films on neutral surfaces were high quality when freshly made, they started to change after 3−4 h. The samples are mounted vertically. It appears that the IL film is flowing down the substrate due to the force of gravity. Therefore, 2D IR measurements were done quickly while the films were still relatively uniform. The amplitude of the signal in the 2D IR experiment was monitored, and the measurement was stopped immediately when the signal started to change. The change in signal indicates a change in the film thickness.

Figure 3 shows 2D IR spectra of the CN stretch of SCN^- taken at T_w = 40 ps for the bulk IL and two ~226 nm thick IL films on substrates with different charge densities, 3.0 and 25.2 nm^{-2}. As mentioned above, the sign of the signal for the bulk sample taken in transmission geometry is opposite of that of the films taken in the near Brewster's angle reflection geometry with an incident angle of 52°, slightly smaller than Brewster's angle,[73] i.e., the bulk band is red (positive going) while the film bands are blue (negative going). The white lines are the center lines. The maximum center line slope is 1, which would occur at T_w = 0 in the absence of any homogeneous broadening.[71,72] Homogeneous broadening reduces the T_w = 0 slope from 1. The difference between 1 and the T_w = 0 slope is a measure of the homogeneous line width.[71] As T_w increases and structural dynamics occur, the initial and final frequencies of the probes within the inhomogeneous line lose correlation, which causes the slope to decrease. At sufficiently long time if complete structural randomization occurs, the slope becomes zero. Therefore, the center line slope at a particular T_w is a measure of the extent of structural evolution of the liquid. As can be seen in Figure 3, the slope for the bulk liquid is significantly smaller than the slopes of the IL films at the same T_w, showing that dynamics in the bulk liquid are faster than in the ~226 nm films.[23,24] Comparing the CLS of the two ~226 nm thick films, it is seen that the film with the surface charge density of 3.0 nm^{-2} has a CLS that is smaller than that of the film with a 25.2 nm^{-2} surface charge density. Therefore, although the films are

https://dx.doi.org/10.1021/jacs.0c03044
J. Am. Chem. Soc. 2020, 142, 9482−9492

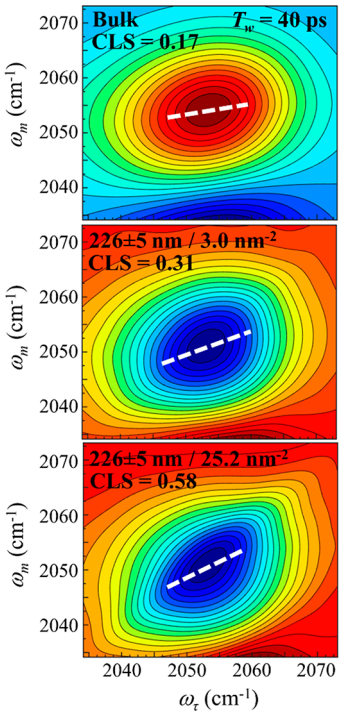

Figure 3. 2D IR spectra at T_w = 40 ps of a bulk sample (top) and 226 nm films on substrates with surface charge densities (cation densities) of 3.0 (middle) and 25.2 nm^{-2} (bottom). The white dashed lines are the center lines. A larger center line slope means that less structural dynamics have occurred in 40 ps.

the same thickness, increasing the charge density slows the structural dynamics.

The CLS(T_w) (the normalized FFCF) taken over a range of T_ws is plotted in Figure 4 for a number of films with

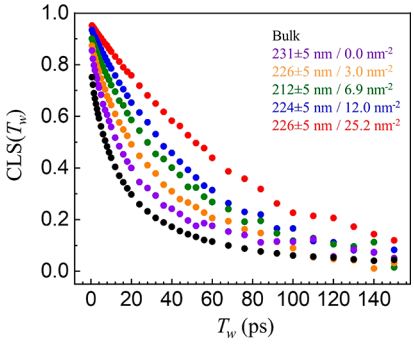

Figure 4. Time dependent CLS(T_w) (normalized frequency-frequency correlation function) of ∼220 nm IL films on substrates with different surface charge densities from 0.0 to 25.2 nm^{-2} and data for the bulk.

thicknesses of ∼220 nm. All of the films have almost the same thickness. The small variation in thicknesses does not have an effect on the decays. However, while the thicknesses of the films are almost the same, the substrates on which the films were spin coated have different charge densities. The CLS(T_w) measured on the bulk IL is also shown. In addition, Figure 4 includes a film spin coated on a surface functionalized only with ethyl (Et), which has 0 surface charge density. As is clear from the figure, as the surface charge density decreases, the dynamics of the film become faster. The IL films on substrates with the neutral surface, Et, have the fastest dynamics but are still slower than the bulk liquid. As shown in Figure 2b,d, the surface charge density (number of bound cations per unit area) can be controlled by the reaction time during the surface functionalization. Therefore, the dynamics of the ionic liquid thin films with the same thicknesses can be changed by the nature of the surface functionalization. In the SI, Figure S1 shows films made on 12 substrates with 12 different surface charge densities. These curves display the same behavior as shown in Figure 4.

To obtain a more quantitative view of the changes in the IL film dynamics with surface charge density, Figure 5 displays the

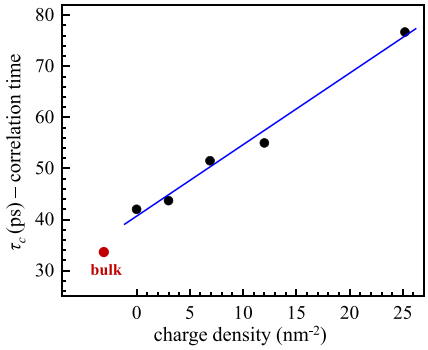

Figure 5. Correlation times (integral of the decay curves), τ_c, for the data in Figure 4 vs the surface charge density. The bulk IL value is also shown (red point). The blue line is a linear fit to the data.

correlation time, τ_c, vs surface charge density obtained from the curves in Figure 4. In addition, a point for the bulk sample was added. τ_c is the integral of the decay curve and is independent of the functional form of the decay. τ_c was obtained by fitting each curve to a sum of exponentials to obtain a good fit. τ_c is then the normalized amplitude of each exponential multiplied by its time constant and summed over all of the exponentials. The fastest two curves were fit with triexponentials, the next curve was fit with a biexponential, and the slowest three curves were fit well with a single exponential. The line is a linear fit to the data. Within the error, the correlation times appear to change linearly with the surface charge density. Figure 5 shows that as the surface charge density increases, for films of the same thickness the film dynamics slow significantly.

To test the reproducibility of the results, films on three substrates that had charge densities of 25.2, 6.9, and 3.0 nm^{-2} were washed off using a methanol flow. The substrates were then sonicated in ethanol and dried under a clean nitrogen flow. Finally a new film of the same thickness was spin coated onto each substrate. The new film on each substrate yielded the same decay curve as the original film.

Figure 4 shows the influence of the surface charge density on films that have almost the same thicknesses. All of the films are ∼220 nm thick. This is relatively thick. Figure 6 shows the effects of changing the surface charge density on three thinner film thicknesses, 50, 90, and 120 nm. For each surface charge density, the same functionalized substrate was used. As discussed immediately above, a substrate with a particular charge density was used to prepare a particular thickness, then cleaned, and used to prepare the next thickness. As can be seen from the three panels in Figure 6, the magnitude of the change

https://dx.doi.org/10.1021/jacs.0c03044
J. Am. Chem. Soc. 2020, 142, 9482−9492

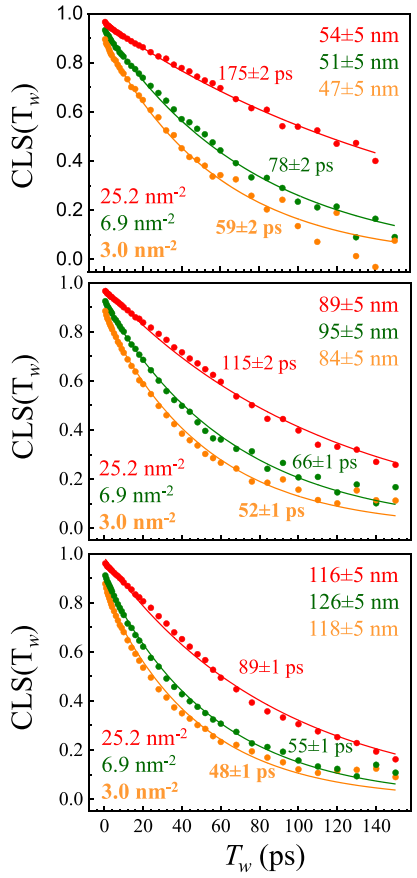

Figure 6. Time dependent CLS(T_w) of ~50 nm (top), ~90 nm (middle), and ~120 nm (bottom) IL films on three substrates that have surface charge densities of 25.2 (red), 6.9 (green), and 3.0 nm^{-2} (orange), respectively. The change in charge density has a larger influence on the film dynamics for thin films. Single-exponential fits and correlation times are also shown in the figure.

in the CLS decays (structural dynamics) becomes greater as the charge density is increased for thinner films.

The influence of the surface charge density as a function of thickness is displayed in Figure 7. The correlation time, τ_c, is plotted as a function of charge density for the three

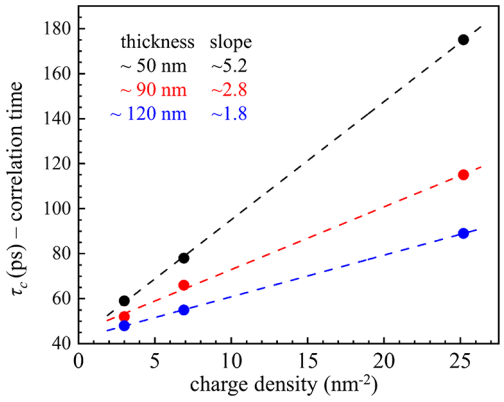

Figure 7. Correlation times (integral of the decay curves), τ_c, for the data in Figure 6 vs the surface charge density. The lines are linear fits to the data. As the film becomes thinner the slope of the line becomes larger, demonstrating that the change in surface charge density has a larger impact for thinner films.

thicknesses. The decay curves in Figure 6 all fit well to single exponentials, so τ_c is the exponential decay constant. The points fall remarkably well on lines, although there are only three charge density values for each thickness. It is clear from the increasing slopes of the lines that changes in the surface change density have a larger effect as the films are made thinner.

In Figure 4, the zero surface charge density curve was obtained by functionalizing the surface with a neutral moiety, Et. Figure 8 shows the CLS(T_w) curves for three IL films of

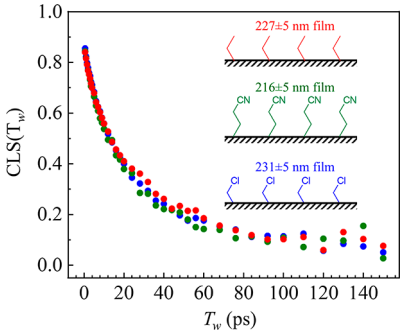

Figure 8. CLS(T_w) for ~225 nm IL films on three neutral substrates with different head groups. The dynamics are independent of the headgroup but distinct from the bulk liquid CLS(T_w) as shown in Figure 4.

almost the same thickness, ~225 nm. The surfaces were functionalized with short alkyl chains with neutral head groups methyl, cynano, and chloro (see Figure 8, insets). The curves are identical within experimental error. Figure 8 shows that the nature of the neutral moiety is not significant. It is the lack of charge that matters. Furthermore, at least for these relatively thick films, the polarity of the headgroup does not matter.

The charge density effects we have observed depend on the extent of functionalization. Almost all or all of the imidazolinium cations must be compensated with anions. As the step 1 functionalization reaction is run for longer time (see Figures 1 and 2), an increasingly thick network of SiO_2/propyl imidazoline is formed. In step 2, the imidazolines are converted into butyl imidazolinium cations. We have defined the surface charge density as the number of imidazolinium cations in the surface bound network per unit surface area (nm^{-2}). When the cation network is formed, prior to spin coating on the IL films, which are thick compared to the surface layer, the counter-anion is I^-. The I^- are undoubtedly eliminated during the spin coating process as there are far more IL NTf_2^- anions than I^- anions. Furthermore, tests show that reusing the same substrate after methodically removing the IL film and spin coating on another film of the same thickness gives the same results. Removing and replacing the film would further dilute out any remaining I^-. Therefore, the anions compensating the butylimidazolinium cations are not I^-.

The spin coated IL layer contains SCN^- in addition to NTf_2^-. Tests were performed to see if SCN^-, which may be in the surface functionalized network layer, has an effect on the results. In addition to the experiments performed on ILs with 1:10 mixtures of BmimSCN and $BmimNTf_2$, experiments were also performed on 1:20 mixtures for both the highest charge density surface and the neutral surface. The data are shown in Figure S2 of the SI. The results for the two SCN^-

https://dx.doi.org/10.1021/jacs.0c03044
J. Am. Chem. Soc. 2020, 142, 9482−9492

concentrations are essentially identical. Therefore, the presence of the SCN^- is not influencing the results.

4. CONCLUDING REMARKS

The intermolecular interactions of a liquid at an interface will inherently be different from those in the bulk liquid. The distinct properties of an interfacial liquid layer will change the properties of the next layer, and the influence of the interface will propagate into the liquid for some distance. In most liquids, this influence dissipates in 1−2 nm.[19−22] Room temperature ionic liquids are different from normal liquids in the distance over which an interface influences the IL properties. This distance can be many tens of nanometers.[23−37]

In this paper, we presented a detailed study of the effect of the properties of the interface on the structural dynamics of thin IL films. The films ranged in thicknesses from 50 to 250 nm. In the study, the SiO_2 surface was functionalized with short alkyl chains with a butylimidazolinium cation headgroup. A sample preparation procedure was developed that allowed reproducible control of the surface charge density, that is, the density of cations. By controlling the reaction time for the initial step in the surface functionalization procedure (see Figures 1 and 2) it was possible to reproducibly form increasingly thick surface network layers of the cations. The structural dynamics of the thin IL films as a function of charge density and thickness were measured with 2D IR spectroscopy. High signal quality for the measurements on thin films was achieved by using near Brewster's angle reflection geometry 2D IR. In addition to the surfaces functionalized with cations, measurements were also presented for surfaces functionalized with three different neutral moieties and the bulk liquid (see Figures 4 and 8). As the surface charge density increased for the same thickness films, the IL dynamics slowed. The fastest dynamics occurred for the neutral surfaces, which still displayed slower dynamics than the bulk liquid. It was also found that the influence of increasing the surface charge density increases as the thickness of the film decreases.

These experiments may have important implications for uses of IL in which a thin layer of liquid near an electrode is involved, e.g., as electrolytes in batteries,[8,9] space craft thrusters,[92] and electrochemically reversible mirrors for space craft.[93] The results show that the properties of the bulk liquid, such as the diffusion constants of solutes, will not be a good guide to the behavior of an IL in a thin layer near an electrode and that the properties can be a function of the electric field.

■ ASSOCIATED CONTENT

Supporting Information

The Supporting Information is available free of charge at https://pubs.acs.org/doi/10.1021/jacs.0c03044.

> Dynamics of IL films on additional substrates; dependence of CLS measurement on probe concentration; procedures of making IL thin films on neutral substrates; flatness characterization of the IL films; effect of different substrate functionalizations on the formation of IL thin films; comparison of the FT-IR spectra of IL films and bulk IL; and Figures S1−S7 (PDF)

■ AUTHOR INFORMATION

Corresponding Author

Michael D. Fayer − *Department of Chemistry, Stanford University, Stanford, California 94305, United States;* orcid.org/0000-0002-0021-1815; Email: fayer@stanford.edu

Authors

Boning Wu − *Department of Chemistry, Stanford University, Stanford, California 94305, United States;* orcid.org/0000-0003-2280-3448

John P. Breen − *Department of Chemistry, Stanford University, Stanford, California 94305, United States*

Xiangyu Xing − *Department of Chemistry, Stanford University, Stanford, California 94305, United States*

Complete contact information is available at: https://pubs.acs.org/10.1021/jacs.0c03044

Notes

The authors declare no competing financial interest.

■ ACKNOWLEDGMENTS

This work was supported by the Air Force Office of Scientific Research Grant No. FA9550-16-1-0104. Part of this work was performed at the Stanford Nano Shared Facilities (SNSF), supported by the National Science Foundation under Award No. ECCS-1542152. We thank Dr. Jun Nishida and Dr. Change Yan for useful suggestions and discussions. We also thank Dr. Rongfeng Yuan for the help with the instrumentation.

■ REFERENCES

(1) Castner, E. W.; Margulis, C. J.; Maroncelli, M.; Wishart, J. F. Ionic Liquids: Structure and Photochemical Reactions. *Annu. Rev. Phys. Chem.* **2011**, *62*, 85−105.

(2) Hayes, R.; Warr, G. G.; Atkin, R. Structure and Nanostructure in Ionic Liquids. *Chem. Rev.* **2015**, *115*, 6357−6426.

(3) Plechkova, N. V.; Seddon, K. R. Applications of ionic liquids in the chemical industry. *Chem. Soc. Rev.* **2008**, *37*, 123−150.

(4) Wishart, J. F. Energy applications of ionic liquids. *Energy Environ. Sci.* **2009**, *2*, 956−961.

(5) MacFarlane, D. R.; Tachikawa, N.; Forsyth, M.; Pringle, J. M.; Howlett, P. C.; Elliott, G. D.; Davis, J. H.; Watanabe, M.; Simon, P.; Angell, C. A. Energy applications of ionic liquids. *Energy Environ. Sci.* **2014**, *7*, 232−250.

(6) Watanabe, M.; Thomas, M. L.; Zhang, S.; Ueno, K.; Yasuda, T.; Dokko, K. Application of Ionic Liquids to Energy Storage and Conversion Materials and Devices. *Chem. Rev.* **2017**, *117*, 7190−7239.

(7) Eshetu, G. G.; Armand, M.; Ohno, H.; Scrosati, B.; Passerini, S. Ionic liquids as tailored media for the synthesis and processing of energy conversion materials. *Energy Environ. Sci.* **2016**, *9*, 49−61.

(8) Xue, L.; Tucker, T. G.; Angell, C. A. Ionic Liquid Redox Catholyte for High Energy Efficiency, Low-Cost Energy Storage. *Adv. Energy Mater.* **2015**, *5*, 1500271.

(9) Lin, M.-C.; Gong, M.; Lu, B.; Wu, Y.; Wang, D.-Y.; Guan, M.; Angell, M.; Chen, C.; Yang, J.; Hwang, B.-J.; Dai, H. An Ultrafast Rechargeable Aluminium-Ion Battery. *Nature* **2015**, *520*, 324−328.

(10) Scovazzo, P.; Visser, A. E.; Davis, J. H.; Rogers, R. D.; Koval, C. A.; DuBois, D. L.; Noble, R. D. Supported Ionic Liquid Membranes and Facilitated Ionic Liquid Membranes. In *Ionic Liquids*; American Chemical Society: Washington, DC, 2002; Vol. *818*, pp 69−87.

(11) Lozano, L. J.; Godínez, C.; de los Ríos, A. P.; Hernández-Fernández, F. J.; Sánchez-Segado, S.; Alguacil, F. J. Recent advances in supported ionic liquid membrane technology. *J. Membr. Sci.* **2011**, *376*, 1−14.

(12) Dai, Z.; Noble, R. D.; Gin, D. L.; Zhang, X.; Deng, L. Combination of ionic liquids with membrane technology: A new approach for CO_2 separation. *J. Membr. Sci.* **2016**, *497*, 1−20.

(13) Fujita, K.; MacFarlane, D. R.; Forsyth, M. Protein solubilising and stabilising ionic liquids. *Chem. Commun.* **2005**, 4804−4806.
(14) Basu, A.; Bhattacharya, S. C.; Kumar, G. S. Influence of the ionic liquid 1-butyl-3-methylimidazolium bromide on amyloid fibrillogenesis in lysozyme: Evidence from photophysical and imaging studies. *Int. J. Biol. Macromol.* **2018**, *107*, 2643−2649.
(15) Parr, D.; Chrestenson, J.; Malik, K.; Molter, M.; Zibart, C.; Egan, B.; Haverhals, L. M. Structure and Dynamics at Ionic Liquid/Electrode Interfaces. *ECS Trans.* **2015**, *66*, 35−42.
(16) Singh, P. C.; Nihonyanagi, S.; Yamaguchi, S.; Tahara, T. Ultrafast Vibrational Dynamics of Water at a Charged Interface Revealed by Two-Dimensional Heterodyne-Detected Vibrational Sum Frequency Generation. *J. Chem. Phys.* **2012**, *137*, 094706.
(17) Hsieh, C. S.; Okuno, M.; Hunger, J.; Backus, E. H.; Nagata, Y.; Bonn, M. Aqueous Heterogeneity at the Air/Water Interface Revealed by 2D-HD-SFG Spectroscopy. *Angew. Chem., Int. Ed.* **2014**, *53*, 8146−8149.
(18) Yan, C.; Thomaz, J. E.; Wang, Y. L.; Nishida, J.; Yuan, R.; Breen, J. P.; Fayer, M. D. Ultrafast to Ultraslow Dynamics of a Langmuir Monolayer at the Air/Water Interface Observed with Reflection Enhanced 2D IR Spectroscopy. *J. Am. Chem. Soc.* **2017**, *139*, 16518−16527.
(19) Moilanen, D. E.; Fenn, E. E.; Wong, D.; Fayer, M. D. Water Dynamics in Large and Small Reverse Micelles: From Two Ensembles to Collective Behavior. *J. Chem. Phys.* **2009**, *131*, 014704.
(20) Fenn, E. E.; Wong, D. B.; Giammanco, C. H.; Fayer, M. D. Dynamics of Water at the Interface in Reverse Micelles: Measurements of Spectral Diffusion with Two-Dimensional Infrared Vibrational Echoes. *J. Phys. Chem. B* **2011**, *115*, 11658−11670.
(21) Coasne, B.; Fourkas, J. T. Structure and Dynamics of Benzene Confined in Silica Nanopores. *J. Phys. Chem. C* **2011**, *115*, 15471−15479.
(22) Yamada, S. A.; Shin, J. Y.; Thompson, W. H.; Fayer, M. D. Water Dynamics in Nanoporous Silica: Ultrafast Vibrational Spectroscopy and Molecular Dynamics Simulations. *J. Phys. Chem. C* **2019**, *123*, 5790−5803.
(23) Nishida, J.; Breen, J. P.; Wu, B.; Fayer, M. D. Extraordinary Slowing of Structural Dynamics in Thin Films of a Room Temperature Ionic Liquid. *ACS Cent. Sci.* **2018**, *4*, 1065−1073.
(24) Wu, B.; Breen, J. P.; Fayer, M. D. Structural Dynamics in Ionic Liquid Thin Films: The Effect of Cation Chain Length. *J. Phys. Chem. C* **2020**, *124*, 4179−4189.
(25) Shin, J. Y.; Yamada, S. A.; Fayer, M. D. Dynamics of a Room Temperature Ionic Liquid in Supported Ionic Liquid Membranes Vs. The Bulk Liquid: 2D IR and Polarized IR Pump-Probe Experiments. *J. Am. Chem. Soc.* **2017**, *139*, 311−323.
(26) Shin, J. Y.; Yamada, S. A.; Fayer, M. D. Carbon Dioxide in a Supported Ionic Liquid Membrane: Structural and Rotational Dynamics Measured with 2D IR and Pump−Probe Experiments. *J. Am. Chem. Soc.* **2017**, *139*, 11222−11232.
(27) Thomaz, J. E.; Bailey, H. E.; Fayer, M. D. The Influence of Mesoscopic Confinement on the Dynamics of Imidazolium-Based Room Temperature Ionic Liquids in Polyether Sulfone Membranes. *J. Chem. Phys.* **2017**, *147*, 194502.
(28) Anaredy, R. S.; Shaw, S. K. Long-Range Ordering of Ionic Liquid Fluid Films. *Langmuir* **2016**, *32*, 5147−5154.
(29) Anaredy, R. S.; Shaw, S. K. Developing Distinct Chemical Environments in Ionic Liquid Films. *J. Phys. Chem. C* **2018**, *122*, 19731−19737.
(30) Anaredy, R. S.; Shaw, S. K. Directing Long-Range Molecular Ordering in Ionic Liquid Films: A Tale of Two Interfaces. *J. Phys. Chem. C* **2019**, *123*, 8975−8982.
(31) Ma, K.; Jarosova, R.; Swain, G. M.; Blanchard, G. J. Charge-Induced Long-Range Order in a Room-Temperature Ionic Liquid. *Langmuir* **2016**, *32*, 9507−9512.
(32) Bovio, S.; Podesta, A.; Lenardi, C.; Milani, P. Evidence of Extended Solidlike Layering in [Bmim][NTf2] Ionic Liquid Thin Films at Room-Temperature. *J. Phys. Chem. B* **2009**, *113*, 6600−6603.
(33) Jurado, L. A.; Kim, H.; Arcifa, A.; Rossi, A.; Leal, C.; Spencer, N. D.; Espinosa-Marzal, R. M. Irreversible Structural Change of a Dry Ionic Liquid under Nanoconfinement. *Phys. Chem. Chem. Phys.* **2015**, *17*, 13613−13624.
(34) Comtet, J.; Niguès, A.; Kaiser, V.; Coasne, B.; Bocquet, L.; Siria, A. Nanoscale capillary freezing of ionic liquids confined between metallic interfaces and the role of electronic screening. *Nat. Mater.* **2017**, *16*, 634−639.
(35) Jiang, W.; Wang, Y.; Yan, T.; Voth, G. A. A Multiscale Coarse-Graining Study of the Liquid/Vacuum Interface of Room-Temperature Ionic Liquids with Alkyl Substituents of Different Lengths. *J. Phys. Chem. C* **2008**, *112*, 1132−1139.
(36) Amith, W. D.; Hettige, J. J.; Castner, E. W.; Margulis, C. J. Structures of Ionic Liquids Having Both Anionic and Cationic Octyl Tails: Lamellar Vacuum Interface vs Sponge-Like Bulk Order. *J. Phys. Chem. Lett.* **2016**, *7*, 3785−3790.
(37) Hettige, J. J.; Amith, W. D.; Castner, E. W.; Margulis, C. J. Ionic Liquids with Symmetric Diether Tails: Bulk and Vacuum-Liquid Interfacial Structures. *J. Phys. Chem. B* **2017**, *121*, 174−179.
(38) Xin, B.; Hao, J. Superhydrophobic Self-Assembled Monolayers of Long-Chain Fluorinated Imidazolium Ionic Liquids. *RSC Adv.* **2012**, *2*, 5141−5146.
(39) Atkin, R.; El Abedin, S. Z.; Hayes, R.; Gasparotto, L. H. S.; Borisenko, N.; Endres, F. AFM and STM Studies on the Surface Interaction of [BMP]TFSA and [EMIm]TFSA Ionic Liquids with Au(111). *J. Phys. Chem. C* **2009**, *113*, 13266−13272.
(40) Hayes, R.; Warr, G. G.; Atkin, R. At the interface: solvation and designing ionic liquids. *Phys. Chem. Chem. Phys.* **2010**, *12*, 1709−1723.
(41) Seddon, J. R. T. Conservative and Dissipative Interactions of Ionic Liquids in Nanoconfinement. *J. Phys. Chem. C* **2014**, *118*, 22197−22201.
(42) Ichii, T.; Negami, M.; Sugimura, H. Atomic-Resolution Imaging on Alkali Halide Surfaces in Viscous Ionic Liquid Using Frequency Modulation Atomic Force Microscopy. *J. Phys. Chem. C* **2014**, *118*, 26803−26807.
(43) Niemann, T.; Li, H.; Warr, G. G.; Ludwig, R.; Atkin, R. Influence of Hydrogen Bonding between Ions of Like Charge on the Ionic Liquid Interfacial Structure at a Mica Surface. *J. Phys. Chem. Lett.* **2019**, *10*, 7368−7373.
(44) Perkin, S.; Crowhurst, L.; Niedermeyer, H.; Welton, T.; Smith, A. M.; Gosvami, N. N. Self-assembly in the electrical double layer of ionic liquids. *Chem. Commun.* **2011**, *47*, 6572−6574.
(45) Smith, A. M.; Lovelock, K. R. J.; Gosvami, N. N.; Licence, P.; Dolan, A.; Welton, T.; Perkin, S. Monolayer to Bilayer Structural Transition in Confined Pyrrolidinium-Based Ionic Liquids. *J. Phys. Chem. Lett.* **2013**, *4*, 378−382.
(46) Espinosa-Marzal, R. M.; Arcifa, A.; Rossi, A.; Spencer, N. D. Microslips to "Avalanches" in Confined, Molecular Layers of Ionic Liquids. *J. Phys. Chem. Lett.* **2014**, *5*, 179−184.
(47) Lhermerout, R.; Perkin, S. A new methodology for a detailed investigation of quantized friction in ionic liquids. *Phys. Chem. Chem. Phys.* **2020**, *22*, 455−466.
(48) Sha, M.; Wu, G.; Dou, Q.; Tang, Z.; Fang, H. Double-Layer Formation of [Bmim][PF6] Ionic Liquid Triggered by Surface Negative Charge. *Langmuir* **2010**, *26*, 12667−12672.
(49) Shimizu, K.; Pensado, A.; Malfreyt, P.; Pádua, A. A. H.; Canongia Lopes, J. N. 2D or not 2D: Structural and charge ordering at the solid-liquid interface of the 1-(2-hydroxyethyl)-3-methylimidazolium tetrafluoroborate ionic liquid. *Faraday Discuss.* **2012**, *154*, 155−169.
(50) Mendonça, A. C. F.; Fomin, Y. D.; Malfreyt, P.; Pádua, A. A. H. Novel ionic lubricants for amorphous carbon surfaces: molecular modeling of the structure and friction. *Soft Matter* **2013**, *9*, 10606−10616.
(51) Wang, Y.-L.; Laaksonen, A.; Lu, Z.-Y. Influence of ionic liquid film thickness on ion pair distributions and orientations at graphene and vacuum interfaces. *Phys. Chem. Chem. Phys.* **2013**, *15*, 13559−13569.

https://dx.doi.org/10.1021/jacs.0c03044
J. Am. Chem. Soc. 2020, 142, 9482−9492

(52) Wang, Y.-L.; Laaksonen, A. Interfacial structure and orientation of confined ionic liquids on charged quartz surfaces. *Phys. Chem. Chem. Phys.* **2014**, *16*, 23329−23339.
(53) Freitas, A. A. d.; Shimizu, K.; Smith, A. M.; Perkin, S.; Canongia Lopes, J. N. Structure and dynamics of mica-confined films of $[C_{10}C_1Pyrr][NTf_2]$ ionic liquid. *J. Chem. Phys.* **2018**, *148*, 193808.
(54) Hayes, R.; Borisenko, N.; Tam, M. K.; Howlett, P. C.; Endres, F.; Atkin, R. Double Layer Structure of Ionic Liquids at the Au(111) Electrode Interface: An Atomic Force Microscopy Investigation. *J. Phys. Chem. C* **2011**, *115*, 6855−6863.
(55) Atkin, R.; Borisenko, N.; Drüschler, M.; El Abedin, S. Z.; Endres, F.; Hayes, R.; Huber, B.; Roling, B. An in situSTM/AFM and impedance spectroscopy study of the extremely pure 1-butyl-1-methylpyrrolidinium tris(pentafluoroethyl)trifluorophosphate/Au(111) interface: potential dependent solvation layers and the herringbone reconstruction. *Phys. Chem. Chem. Phys.* **2011**, *13*, 6849−6857.
(56) Endres, F.; Borisenko, N.; El Abedin, S. Z.; Hayes, R.; Atkin, R. The interface ionic liquid(s)/electrode(s): In situSTM and AFM measurements. *Faraday Discuss.* **2012**, *154*, 221−233.
(57) Yamamoto, R.; Morisaki, H.; Sakata, O.; Shimotani, H.; Yuan, H.; Iwasa, Y.; Kimura, T.; Wakabayashi, Y. External electric field dependence of the structure of the electric double layer at an ionic liquid/Au interface. *Appl. Phys. Lett.* **2012**, *101*, 053122.
(58) Black, J. M.; Walters, D.; Labuda, A.; Feng, G.; Hillesheim, P. C.; Dai, S.; Cummings, P. T.; Kalinin, S. V.; Proksch, R.; Balke, N. Bias-Dependent Molecular-Level Structure of Electrical Double Layer in Ionic Liquid on Graphite. *Nano Lett.* **2013**, *13*, 5954−5960.
(59) Hamm, P.; Zanni, M. T. *Concepts and Methods of 2D Infrared Spectroscopy*; Cambridge University Press: Cambridge, U.K., 2011.
(60) Kraack, J. P.; Hamm, P. Surface-Sensitive and Surface-Specific Ultrafast Two-Dimensional Vibrational Spectroscopy. *Chem. Rev.* **2017**, *117*, 10623−10664.
(61) Daly, C. A.; Brinzer, T.; Allison, C.; Garrett-Roe, S.; Corcelli, S. A. Enthalpic Driving Force for the Selective Absorption of CO2 by an Ionic Liquid. *J. Phys. Chem. Lett.* **2018**, *9*, 1393−1397.
(62) Brinzer, T.; Daly, C. A.; Allison, C.; Garrett-Roe, S.; Corcelli, S. A. Modeling Carbon Dioxide Vibrational Frequencies in Ionic Liquids: III. Dynamics and Spectroscopy. *J. Phys. Chem. B* **2018**, *122*, 8931−8942.
(63) Yamada, S. A.; Bailey, H. E.; Tamimi, A.; Li, C.; Fayer, M. D. Dynamics in a Room-Temperature Ionic Liquid from the Cation Perspective: 2D IR Vibrational Echo Spectroscopy. *J. Am. Chem. Soc.* **2017**, *139*, 2408−2420.
(64) Tamimi, A.; Fayer, M. D. Ionic Liquid Dynamics Measured with 2D IR and IR Pump−Probe Experiments on a Linear Anion and the Influence of Potassium Cations. *J. Phys. Chem. B* **2016**, *120*, 5842−5854.
(65) Kramer, P. L.; Giammanco, C. H.; Fayer, M. D. Dynamics of water, methanol, and ethanol in a room temperature ionic liquid. *J. Chem. Phys.* **2015**, *142*, 212408.
(66) Giammanco, C. H.; Kramer, P. L.; Yamada, S. A.; Nishida, J.; Tamimi, A.; Fayer, M. D. Carbon dioxide in an ionic liquid: Structural and rotational dynamics. *J. Chem. Phys.* **2016**, *144*, 104506.
(67) Pasternack, R. M.; Rivillon Amy, S.; Chabal, Y. J. Attachment of 3-(Aminopropyl)triethoxysilane on Silicon Oxide Surfaces: Dependence on Solution Temperature. *Langmuir* **2008**, *24*, 12963−12971.
(68) Widegren, J. A.; Laesecke, A.; Magee, J. W. The effect of dissolved water on the viscosities of hydrophobic room-temperature ionic liquids. *Chem. Commun.* **2005**, 1610−1612.
(69) Nishida, J.; Breen, J. P.; Lindquist, K. P.; Umeyama, D.; Karunadasa, H. I.; Fayer, M. D. Dynamically Disordered Lattice in a Layered Pb-I-SCN Perovskite Thin Film Probed by Two-Dimensional Infrared Spectroscopy. *J. Am. Chem. Soc.* **2018**, *140*, 9882−9890.
(70) Kubo, R. A Stochastic Theory of Line Shapes. *Adv. Chem. Phys.* **2007**, *15*, 101−127.
(71) Kwak, K.; Park, S.; Finkelstein, I. J.; Fayer, M. D. Frequency-Frequency Correlation Functions and Apodization in Two-Dimensional Infrared Vibrational Echo Spectroscopy: A New Approach. *J. Chem. Phys.* **2007**, *127*, 124503.
(72) Kwak, K.; Rosenfeld, D. E.; Fayer, M. D. Taking Apart the Two-Dimensional Infrared Vibrational Echo Spectra: More Information and Elimination of Distortions. *J. Chem. Phys.* **2008**, *128*, 204505.
(73) Nishida, J.; Yan, C.; Fayer, M. D. Enhanced Nonlinear Spectroscopy for Monolayers and Thin Films in Near-Brewster's Angle Reflection Pump-Probe Geometry. *J. Chem. Phys.* **2017**, *146*, 094201.
(74) Deyko, A.; Cremer, T.; Rietzler, F.; Perkin, S.; Crowhurst, L.; Welton, T.; Steinrück, H.-P.; Maier, F. Interfacial Behavior of Thin Ionic Liquid Films on Mica. *J. Phys. Chem. C* **2013**, *117*, 5101−5111.
(75) Sobota, M.; Nikiforidis, I.; Hieringer, W.; Paape, N.; Happel, M.; Steinrück, H. P.; Görling, A.; Wasserscheid, P.; Laurin, M.; Libuda, J. Toward Ionic-Liquid-Based Model Catalysis: Growth, Orientation, Conformation, and Interaction Mechanism of the $[Tf_2N]-$ Anion in $[Bmim][Tf_2N]$ Thin Films on a Well-Ordered Alumina Surface. *Langmuir* **2010**, *26*, 7199−7207.
(76) Gong, X.; Frankert, S.; Wang, Y.; Li, L. Thickness-dependent molecular arrangement and topography of ultrathin ionic liquid films on a silica surface. *Chem. Commun.* **2013**, *49*, 7803−7805.
(77) Carmichael, A. J.; Hardacre, C.; Holbrey, J. D.; Nieuwenhuyzen, M.; Seddon, K. R. Molecular Layering and Local Order in Thin Films of 1-Alkyl-3-Methylimidazolium Ionic Liquids Using X-Ray Reflectivity. *Mol. Phys.* **2001**, *99*, 795−800.
(78) Maruyama, S.; Takeyama, Y.; Taniguchi, H.; Fukumoto, H.; Itoh, M.; Kumigashira, H.; Oshima, M.; Yamamoto, T.; Matsumoto, Y. Molecular Beam Deposition of Nanoscale Ionic Liquids in Ultrahigh Vacuum. *ACS Nano* **2010**, *4*, 5946−5952.
(79) Cremer, T.; Killian, M.; Gottfried, J. M.; Paape, N.; Wasserscheid, P.; Maier, F.; Steinrück, H. P. Physical Vapor Deposition of $[Emim][Tf_2N]$: A New Approach to the Modification of Surface Properties with Ultrathin Ionic Liquid Films. *ChemPhysChem* **2008**, *9*, 2185−2190.
(80) Cremer, T.; Stark, M.; Deyko, A.; Steinrück, H. P.; Maier, F. Liquid/Solid Interface of Ultrathin Ionic Liquid Films: $[C_1C_1Im]$-$[Tf_2N]$ and $[C_8C_1Im][Tf_2N]$ on Au(111). *Langmuir* **2011**, *27*, 3662−3671.
(81) Schernich, S.; Kostyshyn, D.; Wagner, V.; Taccardi, N.; Laurin, M.; Wasserscheid, P.; Libuda, J. Interactions Between the Room-Temperature Ionic Liquid $[C_2C_1Im][OTf]$ and Pd(111), Well-Ordered Al_2O_3, and Supported Pd Model Catalysts from IR Spectroscopy. *J. Phys. Chem. C* **2014**, *118*, 3188−3193.
(82) Rietzler, F.; Piermaier, M.; Deyko, A.; Steinrück, H.-P.; Maier, F. Electrospray Ionization Deposition of Ultrathin Ionic Liquid Films: $[C_8C_1Im]Cl$ and $[C_8C_1Im][Tf_2N]$ on Au(111). *Langmuir* **2014**, *30*, 1063−1071.
(83) Schernich, S.; Wagner, V.; Taccardi, N.; Wasserscheid, P.; Laurin, M.; Libuda, J. Interface Controls Spontaneous Crystallization in Thin Films of the Ionic Liquid $[C_2C_1Im][OTf]$ on Atomically Clean Pd(111). *Langmuir* **2014**, *30*, 6846−6851.
(84) Biedron, A. B.; Garfunkel, E. L.; Castner, E. W.; Rangan, S. Ionic Liquid Ultrathin Films at the Surface of Cu (100) and Au (111). *J. Chem. Phys.* **2017**, *146*, 054704.
(85) Lexow, M.; Heller, B. S. J.; Maier, F.; Steinrück, H.-P. Anion Exchange at the Liquid/Solid Interface of Ultrathin Ionic Liquid Films on Ag(111). *ChemPhysChem* **2018**, *19*, 2978−2984.
(86) Höfft, O.; Bahr, S.; Kempter, V. Investigations with Infrared Spectroscopy on Films of the Ionic Liquid $[EMIM]Tf_2N$. *Langmuir* **2008**, *24*, 11562−11566.
(87) Peanasky, J.; Schneider, H. M.; Granick, S.; Kessel, C. R. Self-Assembled Monolayers on Mica for Experiments Utilizing the Surface Forces Apparatus. *Langmuir* **1995**, *11*, 953−962.
(88) Yoshida, W.; Castro, R. P.; Jou, J.-D.; Cohen, Y. Multilayer Alkoxysilane Silylation of Oxide Surfaces. *Langmuir* **2001**, *17*, 5882−5888.
(89) Vandenberg, E. T.; Bertilsson, L.; Liedberg, B.; Uvdal, K.; Erlandsson, R.; Elwing, H.; Lundström, I. Structure of 3-aminopropyl

https://dx.doi.org/10.1021/jacs.0c03044
J. Am. Chem. Soc. 2020, 142, 9482−9492

triethoxy silane on silicon oxide. *J. Colloid Interface Sci.* **1991**, *147*, 103−118.
(90) Nishiyama, N.; Ishizaki, T.; Horie, K.; Tomari, M.; Someya, M. Novel polyfunctional silanes for improved hydrolytic stability at the polymer−silica interface. *J. Biomed. Mater. Res.* **1991**, *25*, 213−221.
(91) Gunda, N. S. K.; Singh, M.; Norman, L.; Kaur, K.; Mitra, S. K. Optimization and characterization of biomolecule immobilization on silicon substrates using (3-aminopropyl)triethoxysilane (APTES) and glutaraldehyde linker. *Appl. Surf. Sci.* **2014**, *305*, 522−530.
(92) Prince, B. D.; Fritz, B. A.; Chiu, Y.-H. Ionic Liquids in Electrospray Propulsion Systems. In *Ionic Liquids: Science and Applications*; American Chemical Society: Washington, DC, 2012; Vol. *1117*, pp 27−50.
(93) Dziedzic, R. M.; Waddington, M. A.; Lee, S. E.; Kleinsasser, J.; Plumley, J. B.; Ewing, W. C.; Bosley, B. D.; Lavallo, V.; Peng, T. L.; Spokoyny, A. M. Reversible Silver Electrodeposition from Boron Cluster Ionic Liquid (Bcil) Electrolytes. *ACS Appl. Mater. Interfaces* **2018**, *10*, 6825−6830.

https://dx.doi.org/10.1021/jacs.0c03044
J. Am. Chem. Soc. 2020, 142, 9482−9492